| Title | True photoluminescence spectra revealed in electrospun light-emitting single nanofibers |
|---|---|
| Author(s) | Ishii, Yuya; Murata, Hideyuki |
| Citation | Journal of Materials Chemistry, 22(11): 4695-4703 |
| Issue Date | 2012-01-26 |
| Type | Journal Article |
| Text version | author |
| URL | http://hdl.handle.net/10119/10873 |
| Rights | Copyright (C) 2012 Royal Society of Chemistry. Yuya Ishii and Hideyuki Murata, Journal of Materials Chemistry, 22(11), 2012, 4695-4703. http://dx.doi.org/10.1039/C2JM14831E - Reproduced by permission of The Royal Society of Chemistry |
| Description | |

JAIST
JAPAN
ADVANCED INSTITUTE OF
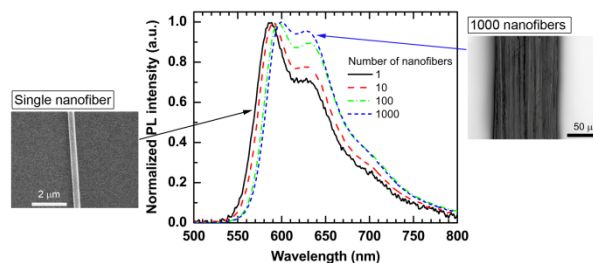SCIENCE AND TECHNOLOGY

Japan Advanced Institute of Science and Technology

**Full paper**

# True photoluminescence spectra revealed in electrospun light-emitting single nanofibers

**Yuya Ishii, and Hideyuki Murata***

We demonstrate for the first time that number and packing of electrospun light-emitting nanofibers significantly affect to the shape of PL spectra.

We demonstrate for the first time that re-absorption and scatterings of photoluminescence (PL) significantly occurs among electrospun light-emitting nanofibers. Electrospun nanofibers composed of a
10 blend of poly[2-methoxy-5-(2′-ethyl-hexyloxy)-1,4-phenylenevinylene] and poly(ethylene oxide) with and without LiCF$_3$SO$_3$ were prepared in controlled numbers. Different numbers of fibers showed different PL spectra even though the PL spectra from individual fibers were almost the same. Results of simulated PL spectra using UV-vis absorption spectra measured with and without an integrating sphere revealed that the change of PL spectral is due to re-absorption and scatterings of PL among the fibers. Although
15 most PL spectra of electrospun nanofibers have been performed with a sheet or mat of many electrospun fibers, our study clearly shows that measuring PL spectrum of a single fiber is indispensable for precisely evaluating the aggregation states and the electronic states of conjugated polymers inside the fibers.

## Introduction

Electrospun fibers consisting of conjugated polymers have the
20 potential to realize high-performance optoelectronic devices, such as transistors, light-emitting diodes, and photo- or chemical sensors; this is because the fibers have a diameter in the nanometer range, and the polymer chains inside the fibers are aligned along the fiber direction [1-3]. Recently, several studies
25 have revealed unique properties of electrospun nanofibers compared to their thin films, such as enhanced electrical or proton conductivity [4, 5], carrier mobility [6, 7], polarized photoluminescence (PL) [8, 9], and highly-efficient electroluminescence [10]. These properties are further enhanced by
30 uniaxial alignment of the fibers since conjugated polymers inside the fibers are oriented along the alignment direction.

The aggregation states of conjugated polymer chains are known to affect the properties of the above-mentioned devices [11, 12] as a reflection of their alignments. Blending conjugated and
35 nonconjugated polymers is an effective way to control the aggregation states of conjugated polymer chains. The blended films show improved properties, such as enhanced carrier mobility and stability [13] and higher electroluminescence efficiency [14], compared to pure conjugated polymer films. PL
40 measurements provide information significant to evaluating the aggregation states [15-18]. Many studies have focused on measuring the PL from electrospun nanofibers composed of blends to evaluate the aggregation states of the conjugated polymers inside the fibers. In these studies, random mats or aligned sheets
45 consisting of many fibers are measured. However, the PL spectra from these mats or sheets not only reflect the PL spectra from individual fibers but may also be affected by optical effects among the fibers, which are re-absorption and scatterings among the fibers including Rayleigh, Mie and geometric scatterings.
50 In this study, we found number and packing of electrospun fibers significantly affects PL spectra due to re-absorption and scatterings among the fibers for the first time. Here, we demonstrate the importance of measuring the PL of a single fiber for precise evaluation of the aggregation states and the electronic
55 states of the conjugated polymer chains. We have successfully discussed the aggregation and electronic states of the conjugated polymer chains nanoconfined inside the nanofibers.

## Experiments

### Materials

Poly[2-methoxy-5-(2′-ethyl-hexyloxy)-1,4-phenylenevinylene] (MEH-PPV) is a widely used light-emitting polymer in the field of organic light-emitting diodes. Poly(ethylene oxide) (PEO) was chosen as an electrospinnable polymer since it is known to be easily electrospun and relatively soluble in chloroform, which is good solvent for MEH-PPV. MEH-PPV ($Mn$ = 150,000–250,000), PEO ($Mv$ = 8,000,000 and $Mv$ = 400,000), and $LiCF_3SO_3$ (99.995%) were purchased from Aldrich and used as received. High molecular weight (HMW) PEO was used for MEH-PPV/PEO(HMW)/$LiCF_3SO_3$ fibers and their spin-coated films, and low molecular weight (LMW) PEO was used for MEH-PPV/PEO(LMW) fibers and their spin-coated films. We used HMW PEO for the MEH-PPV/PEO(HMW)/$LiCF_3SO_3$ fibers since using LMW PEO didn't give us stable fibers. Chloroform (99.0%) and cyclohexanone (99.0%) were purchased from Kanto Chemical Co., Inc., and used as received.

For MEH-PPV/PEO(HMW)/$LiCF_3SO_3$ fibers and the films, MEH-PPV (15 mg) and PEO(HMW) (30 mg) were dissolved in chloroform (3734 μl), and $LiCF_3SO_3$ was dissolved separately in cyclohexanone at a concentration of 20 mg·ml$^{-1}$. Then, 266 μl of the $LiCF_3SO_3$ solution was added to the MEH-PPV/PEO(HMW) solution and mixed by a magnetic stirrer at room temperature for 5 min. The mass ratio of the resulting solution was set at MEH-PPV:PEO(HMW):$LiCF_3SO_3$ = 1:2:0.36. For MEH-PPV/PEO(LMW) fibers and the films, MEH-PPV (40 mg) and PEO(LMW) (80 mg) were dissolved in chloroform (4000 μl). The mass ratio of the resulting solution was set at MEH-PPV:PEO(LMW) = 1:2.

### Electrospun fibers

The blend solution of MEH-PPV/PEO(HMW)/$LiCF_3SO_3$ or MEH-PPV/PEO(LMW) was loaded into a glass syringe equipped with a stainless steel needle (0.3 mm in diameter). The solution was continuously supplied using a syringe pump (KDS-100, KD scientific Inc.) at a rate of 0.18 ml·h$^{-1}$ for the MEH-PPV/PEO(HMW)/$LiCF_3SO_3$ solution or 0.20 ml·h$^{-1}$ for MEH-PPV/PEO(LMW) solution. The needle was connected to a high-voltage power supply (HVU-30P100, Mecc Co., Ltd.). The distance between the needle and collectors, which were composed of two pieces of stainless steel, was fixed at 10 cm. The voltage applied to the needle was 2.0 kV for the MEH-PPV/PEO(HMW)/$LiCF_3SO_3$ solution and 2.8 kV for the MEH-PPV/PEO(LMW) solution. Full details on the fabrication of number-controlled aligned fibers are given elsewhere [19]. Briefly, one of the two collectors was biased with a negative voltage (-800 V), while the other collector was grounded. Electrospun fibers were selectively deposited onto the negatively biased collector, which was alternated by a switching electrode unit (Mecc Co., Ltd.). Depending on the switching cycle, number-controlled and aligned fibers were formed that bridged the two collectors. All of the electrospinning experiments were performed in air at room temperature with a humidity of 30%–49%. The produced fibers were transferred to U-shaped holders upon which the fibers were bridged at both edges. The fibers were then vacuum-dried for 7 h to remove the solvents.

### Spin-coated films

Thin film samples were prepared by spin-coating the blended solutions on cleaned quartz substrates in air at room temperature. To prepare thin films with different thicknesses, we spin-coated them at different spinning speeds (1000–7000 rpm for 90 s). The films were then vacuum-dried for 7 h to remove the solvents.

### Characterization method

Shapes and diameters of the fibers were characterized by means of a scanning electron microscope (SEM, S-4100, Hitachi), laser scanning microscope (VK-9700, Keyence), and fluorescence microscope (BZ-8000, Keyence). The average diameters of the fibers were calculated from 100 SEM images of the individual fibers (2 images per each 50 individual fibers). The average diameter using this dataset mainly represents distribution of the diameters among fibers. Note that the standard deviation of the fiber diameters among electrospun fibres was about two times larger than that within an individual fiber [20]. Film thickness was measured by an atomic force microscope (VN-8000, Keyence), and an average film thickness was calculated by measuring 25 positions on a film.

PL spectra were measured using a homemade setup. Excitation light at 460 nm was supplied by a light source (Optical ModuleX, Ushio Inc.) coupled with a grating monochromator (T-25C, JASCO). The PL spectra from the samples were collected 50° against the excitation light with a spectral analyzer (PMA-11, Hamamatsu) through a sharp-cut filter ($\lambda > 500$ nm). Thin films on substrates were placed 90° against the excitation light. The detection area was a circle with a diameter of around 4.2 mm; this was calculated from the numerical aperture of a detection optical fiber equipped on the spectral analyzer.

The absorption spectra of the spin-coated films and dilute solutions were measured with an UV-Vis spectrophotometer (V-670, JASCO). We measured UV-Vis spectra with and without an integrating sphere (ISN-470, JASCO) which can correct scattered lights in absorption spectra. To prepare a dilute solution of MEH-PPV/PEO(HMW)/$LiCF_3SO_3$, MEH-PPV (20 mg), PEO(HMW) (40 mg), and $LiCF_3SO_3$ (7 mg) were dissolved in a mixture of chloroform (1867 ml) and cyclohexanone (133 ml).

## Results and discussion

### Electrospun fibers

When multiple electrospun MEH-PPV/PEO(HMW)/$LiCF_3SO_3$ fibers were deposited on the two collectors by switching the negative voltage, a bundle of the fibers was formed (Fig. 1A). In contrast, multiple MEH-PPV/PEO(LMW) fibers formed in the shape of a sheet (Fig. 1B). This difference is due to the difference in conductivity of the two blends. The blends of MEH-PPV/PEO(HMW)/$LiCF_3SO_3$ have higher conductivity than that of MEH-PPV/PEO(LMW)[21]; this is due to the electrochemical doping of MEH-PPV by $LiCF_3SO_3$ [21-23] or ionic conduction of Li ions in a PEO matrix [24]. This higher conductivity of MEH-PPV/PEO(HMW)/$LiCF_3SO_3$ allows their fibers to release positive charges accumulated in the electrospinning process. In addition, the fibers can be charged negatively by the negatively biased collector. In this situation, fibers are deposited as a bundle. In contrast, electrospun MEH-PPV/PEO(LMW) fibers keep
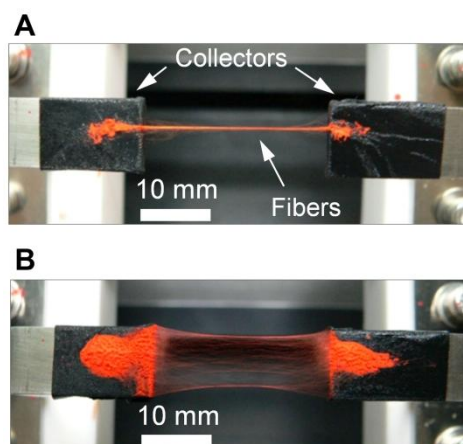
**Fig. 1** One thousand electrospun fibers of A) MEH-PPV/PEO(HMW)/LiCF₃SO₃ and B) MEH-PPV/PEO(LMW).
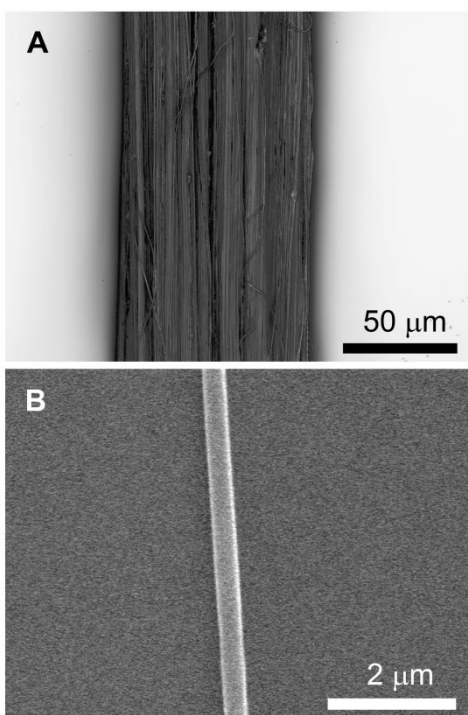


5 **Fig. 2** A) Laser scanning microscope image of 1000 electrospun fibers of MEH-PPV/PEO(HMW)/LiCF₃SO₃. B) SEM image of an electrospun single fiber of MEH-PPV/PEO(HMW)/LiCF₃SO₃.

positive charges on the surface due to their low conductivity, which causes mutual electrostatic repulsion among the fibers [25].
10 In this case, the fibers form a sheet.

Figure 2A shows a laser scanning microscope image of 1000 electrospun fibers of MEH-PPV/PEO(HMW)/LiCF₃SO₃. The formation of a single bundle consisting of the fibers was clearly observed. Individual fibers in the bundle were uniaxially aligned
15 to the bundle direction. A single fiber was produced with a good reproducibility (Fig. 2B). The fiber showed uniaxial alignment and a smooth surface. The average diameter of the fibers was 399 nm with a standard deviation of 73 nm.

Figure 3A shows the fluorescence microscope image of 1000
20 electrospun fibers of MEH-PPV/PEO(LMW) with twofold post-drawing which was done in order to reduce variation in the photoluminescence (PL) spectra among individual electrospun
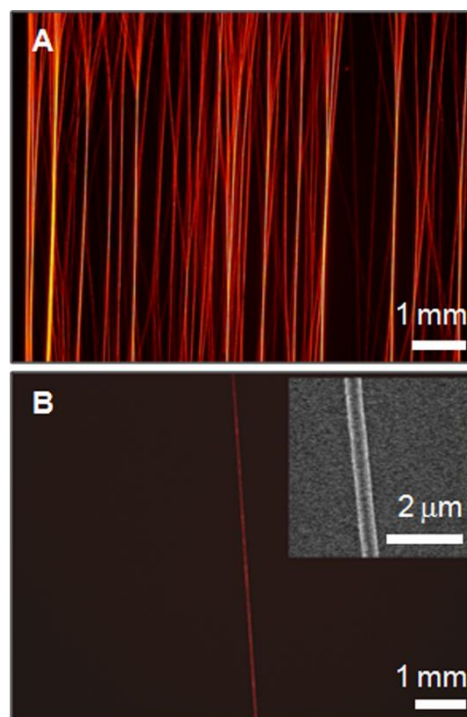


**Fig. 3** Fluorescence microscope images of A) 1000 fibers and B) a single
25 electrospun fiber of MEH-PPV/PEO(LMW). Inset shows a SEM image of a single electrospun fiber of MEH-PPV/PEO(LMW). These electrospun fibers were drawn twofold after electrospinning.

fibers. Details are discussed in section *Photoluminescence (PL) characteristics*. Although the electrospun MEH-PPV/PEO fibers
30 are clearly separated compared to the bundle of MEH-PPV/PEO(HMW)/LiCF₃SO₃ fibers, some of the former are tied together. The average diameter of the undrawn single fibers was 579 nm with a standard deviation of 101 nm, and the average diameter was reduced to 482 nm with a standard deviation of 105
35 nm after twofold post-drawing (Fig. 3B).

**Photoluminescence characteristics**

For PL measurement of a single fiber, ten single MEH-PPV/PEO(HMW)/LiCF₃SO₃ fibers and seven single MEH-PPV/PEO(LMW) fibers were measured individually to confirm
40 the spectrum variation among single electrospun fibers. The single MEH-PPV/PEO(HMW)/LiCF₃SO₃ fibers showed identical PL spectra (Fig. 4). On the other hand, the single MEH-PPV/PEO(LMW) fibers showed different PL spectra compared to the single MEH-PPV/PEO(HMW)/LiCF₃SO₃ fibers (Fig. 5A).
45 This spectral change is due to different aggregation states of MEH-PPV chains inside the MEH-PPV/PEO(LMW) fibers resulting from unstable formation of MEH-PPV/PEO(LMW) fibers during the electrospinning process [26-28]. We can effectively suppress the spectra variation by twofold post-drawing (Fig. 5B).
50 This suppression of the spectra variation after the post-drawing is a prominent finding and suggests improved homogeneity of the aggregation states of MEH-PPV chains. The mechanism of the improvement is not clearly understood yet. However, it may be related to improved uniformity in electronic structure of MEH-
55 PPV chains due to post-drawing[29]. We will discuss this possibility in the later section of *PL spectra from single fibers*.
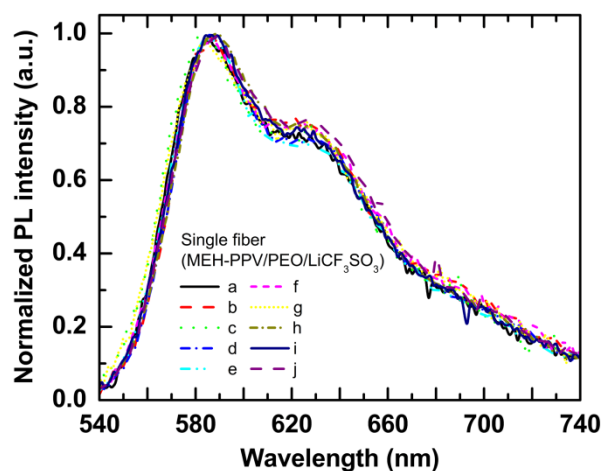
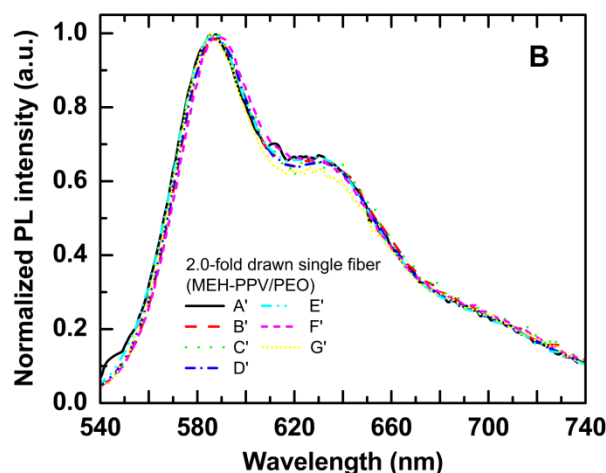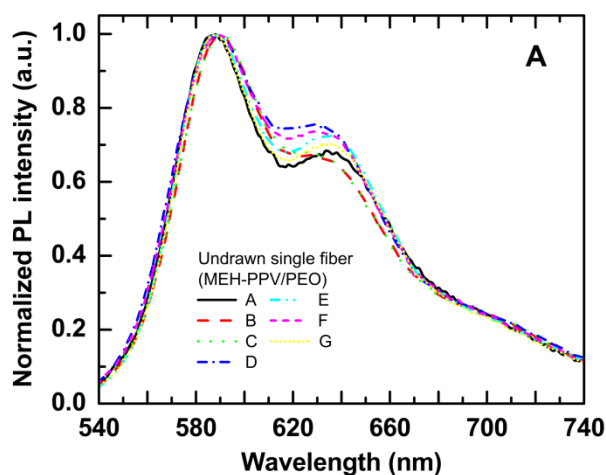**Fig. 4** Normalized PL spectra of ten single fibers of MEH-PPV /PEO(HMW)/LiCF$_3$SO$_3$.





₅ **Fig. 5** Normalized PL spectra of seven single fibers of MEH-PPV/ PEO(LMW) without post-drawing A) and with twofold post-drawing B).





₁₅ **Fig. 6** Normalized PL spectra of different numbers of electrospun fibers: A) An undrawn bundle of MEH-PPV/PEO(HMW)/LiCF$_3$SO$_3$ fibers and B) a twofold drawn sheet of MEH-PPV/PEO(LMW) fibers.

We prepared different numbers of electrospun nanofibers (1, 10, 100, and 1000) and measured their PL spectra. The PL spectra from different numbers of fibers showed different spectra in both ₁₀ cases of a bundle of fibers and a sheet of fibers (Fig. 6). For instance, the emission edge was red-shifted, and the relative intensity for wavelengths longer than 600 nm increased with the number 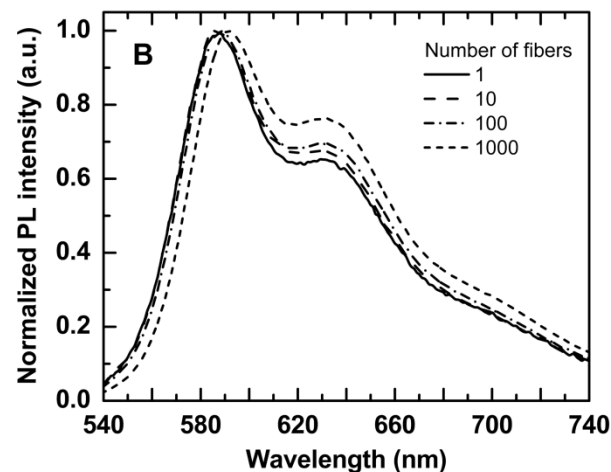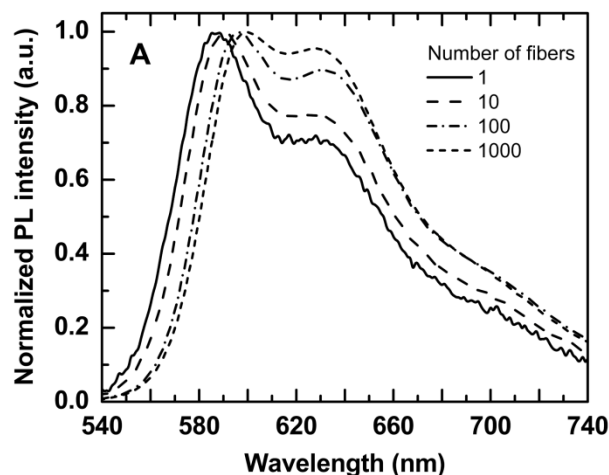of fibers. Since we confirmed that individual fibers show identical spectra, this spectral change in the bundle and the sheet suggests structural effects among the fibers including re-₂₀ absorption and scatterings. From Fig. 6, we also found that PL spectra of the bundles significantly changed with increasing in the number of fibers compared with that of the sheet.

**Re-absorption and scatterings of photoluminescence**

To evaluate the re-absorption and scatterings of PL, we ₂₅ measured the UV-vis absorption spectra of spin-coated films with and without an integrating sphere, which can reduce the contribution of scattered light in absorption spectra. Figure 7 shows UV-vis absorption spectra of a MEH-PPV/PEO(HMW)/LiCF$_3$SO$_3$ spin-coated film with an average ₃₀ thickness of 382 nm. A UV-vis absorption spectrum of a MEH-PPV/PEO(HMW)/LiCF$_3$SO$_3$ dilute solution measured using an integrating sphere was also shown in this figure. Absorption edge of the dilute solution was observed at around 560 nm, whereas that of the films shifted to around 595 nm. At the wavelength ₃₅ longer than 590 nm, absorbance of the dilute solution was negligible. On contrary, absorbance of the films at 590 nm was observed and gradually decreased with increasing the wavelength. This is mainly due to scatterings of incident light[30, 31] because, the absorption spectrum of the film measured with an integrating ₄₀ sphere clearly reduced the absorbance at the wavelength longer
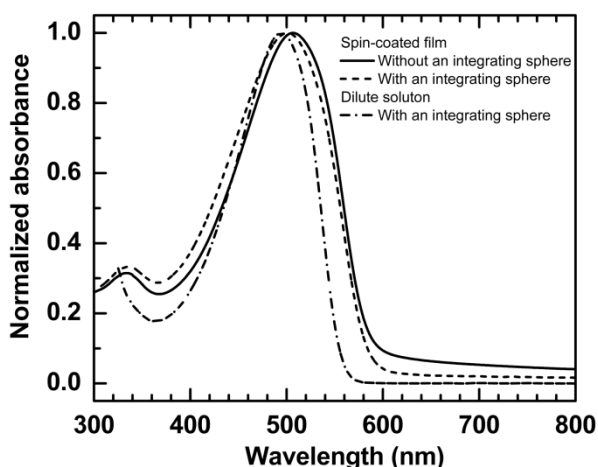
**Fig. 7** Normalized UV-vis absorption spectra of a MEH-PPV/PEO(HMW)/LiCF$_3$SO$_3$ spin-coated film measured with and without an integrating sphere. Average thickness of the film is 382 nm. The spectrum of a MEH-PPV/PEO(HMW)/LiCF$_3$SO$_3$ dilute solution measured with an integrating sphere is also shown.
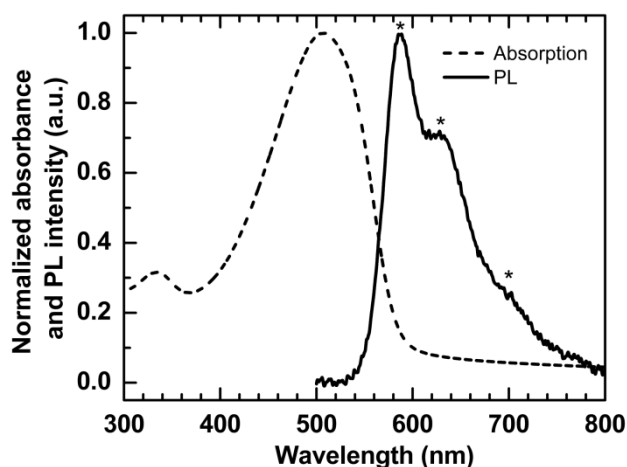


**Fig. 8** Normalized UV-vis absorption spectrum of a MEH-PPV/PEO(HMW)/LiCF$_3$SO$_3$ spin-coated film (thickness 382 nm) measured without an integrating sphere and a normalized PL spectrum of a single MEH-PPV/PEO(HMW)/LiCF$_3$SO$_3$ fiber.

than 590 nm. This result is also indicative of the fact that the UV-vis absorption spectra measured without integrating sphere includes not only true absorption by the films but also scatterings of incident light. Thus, we use UV-vis absorption spectra measured without an integrating sphere to include the scattering effect for the simulation of PL spectra (*vide infra*) which explains why the PL spectra from different numbers of fibers showed different spectra.

Figure 8 shows the UV-vis absorption spectrum of a MEH-PPV/PEO(HMW)/LiCF$_3$SO$_3$ spin-coated film measured without an integrating sphere and the PL spectrum from a single MEH-PPV/PEO(HMW)/LiCF$_3$SO$_3$ fiber. Both of the spectra were normalized to each of their peak values. The UV-vis absorption spectrum largely overlapped with the PL spectrum at 530–600 nm. Therefore, re-absorption and scatterings easily occurs in PL with an increase in the number of the fibers. In order to confirm how much re-absorption and scatterings affect to the PL spectra, we used a simple model where the PL from a single fiber goes through a film with a thickness of *h* (Fig. 9A). We measured the UV-vis absorption spectra of the spin-coated films with different film thicknesses without an integrating sphere (Fig. 9B). Absorbance increased with film thickness. To demonstrate the re-absorption and scattering effects at different wavelengths, we chose absorbance at 590, 630, and 700 nm, which correspond to the peak and shoulders in the PL spectra of the single MEH-PPV/PEO(HMW)/LiCF$_3$SO$_3$ fibers. We measured the absorbance at these wavelengths and calculated an apparent absorbance. Figure 9C shows the average absorbance from three different measurements as a function of film thickness. The apparent absorbance at 590 nm increased linearly with increasing film thickness and the absorbance at the thickness of 0 nm reach to 0, which agrees well with the Lambert-Beer law: $A = \varepsilon dh$. Here, A, $\varepsilon$, *d*, and *h* are the absorbance, molar absorption coefficient, density of materials, and film thickness, respectively.. On the other hand, the absorbance at 630 nm and 700 nm did not reach to 0 when the thickness was extrapolated to 0 nm. This result confirms that the apparent absorbance at these wavelengths is due to scatterings. We fitted these plots with linear functions, and the equations of the fits are shown in Fig. 9C. From these equations, we calculated the apparent transmittance as a function of film thickness at the wavelengths of 590, 630, and 700 nm. As shown in Fig. 9D, the transmittance at 590 nm significantly decreased with increasing film thickness compared to the transmittances at 630 and 700 nm. For example, at a film thickness of 1200 nm, the transmittances of the film were 52.3% (590 nm), 73.6% (630 nm), and 81.6% (700 nm). The larger decrease in transmittance at 590 nm would due to re-absorption and scatterings, and moderate decreases in transmittances at 630 nm and 700 nm were ascribed to scatterings among fibers.

To fully understand the changes in PL spectra with increase in the number of fibers, we simulated PL spectra with different thicknesses considering the re-absorption and scatterings. To simulate entire PL spectra for the wavelength range of 540–740 nm, the average absorbance as a function of the average film thickness was fitted to a linear function for the wavelength range of 540–740 nm with a 1-nm step. From the fitted equations at each wavelength, the apparent transmission spectra as a function of film thickness were calculated. Multiplying a PL spectrum of a single fiber by the transmission spectrum brings about the simulated PL spectra composed of different numbers of fibers (Fig. 10). The simulated PL spectra agreed well with the PL spectra of samples with different numbers of fibers. On the other hand, when we use the absorption spectra measured with an integrating sphere, the simulated PL spectra did not match to the experimental results. This result clearly shows that the spectral change in PL is due to re-absorption and scatterings among the fibers. Therefore, measuring the PL spectrum from a single fiber is crucial to see the "true" spectra and indispensable to precisely evaluating the aggregation and the electronic states of conjugated polymers inside the fibers.

The film thicknesses employed for the simulation shown in Fig. 10 were effective thicknesses reproducing the PL spectra observed in the fiber samples. The simulated thicknesses seemed to be much smaller than the size of a bundle or sheet of fibers. This is due to voids among the fibers. The film thicknesses used for the simulated PL spectra of the bundle were thicker than
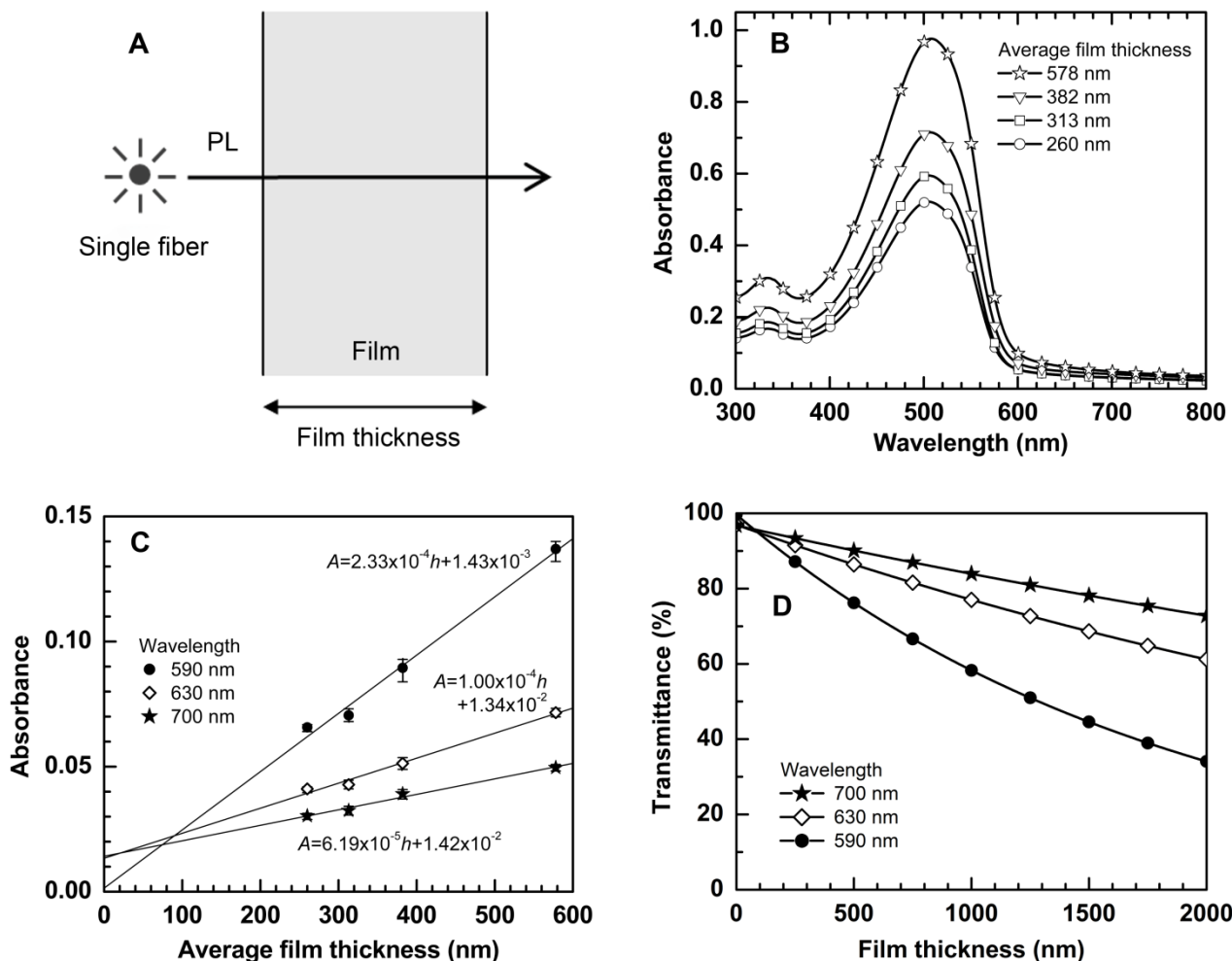
**Fig. 9** A) Schematic illustration of a model evaluating PL spectral change due to self-absorption and scatterings. B) UV-vis absorption spectra of MEH-PPV/PEO(HMW)/LiCF$_3$SO$_3$ spin-coated films with different film thicknesses, which were measured without an integrating sphere. C) Absorbance at three different wavelengths as a function of MEH-PPV/PEO(HMW)/LiCF$_3$SO$_3$ film thickness. Errors reflect maximum and minimum values. Plots are fitted by linear functions (solid lines). D) Transmittance as a function of MEH-PPV/PEO(HMW)/LiCF$_3$SO$_3$ film thickness, which is calculated from the fitted equations.

those for the sheet. This result suggests that greater re-absorption and scatterings takes place in bundles of the fibers. To confirm the effect of packing of fibers on the shape of PL spectra, we measured PL spectra of a sheet of 1000 MEH-PPV/PEO(LMW) fibers with twofold post-drawing (Figs. 11A and 11C). Then, the sheet of the fibers was gathered with a U-shape wire (Fig. 11B) to fabricate a bundle (Fig. 11D). The PL spectrum of the bundle red-shifted significantly with a reduction of PL intensity at wavelength of shorter than 595 nm and a relative increase in the intensity at 630 nm. (Fig. 11E) This result clearly shows close packing of fibers affects to the shape of PL spectra.

We also performed a simulation of PL spectra using UV-vis absorption spectra of spin-coated films measured with an integrating sphere (Fig. 12). We chose thicknesses for the simulation as the intensities of PL are comparable at a wavelength of 630 nm. The simulated spectra was inconsistent with the PL spectra of the 1000 fibers; lower intensity in the simulated spectra was observed at the wavelength of shorter than 590 nm and longer than 630 nm. This result is an evidence of that

the scatterings plays important role in the shape of PL spectra composed of many fibers.

We consider this simulation is an initial step to explain the PL spectra of multiple fiber samples. A detail analysis will be necessary for complete simulation of PL spectra by taking into account of several kinds of scattering modes based on Rayleigh theory, Mie theory and a cylindrical geometry of the electrospun fibers[32]. Nevertheless, we could clearly demonstrate that different number and packing of electrospun nanofibers show different PL spectra and measuring the PL spectrum from a single fiber is indispensable especially for precisely evaluating the aggregation states and the electronic states of conjugated polymers inside the fibers.
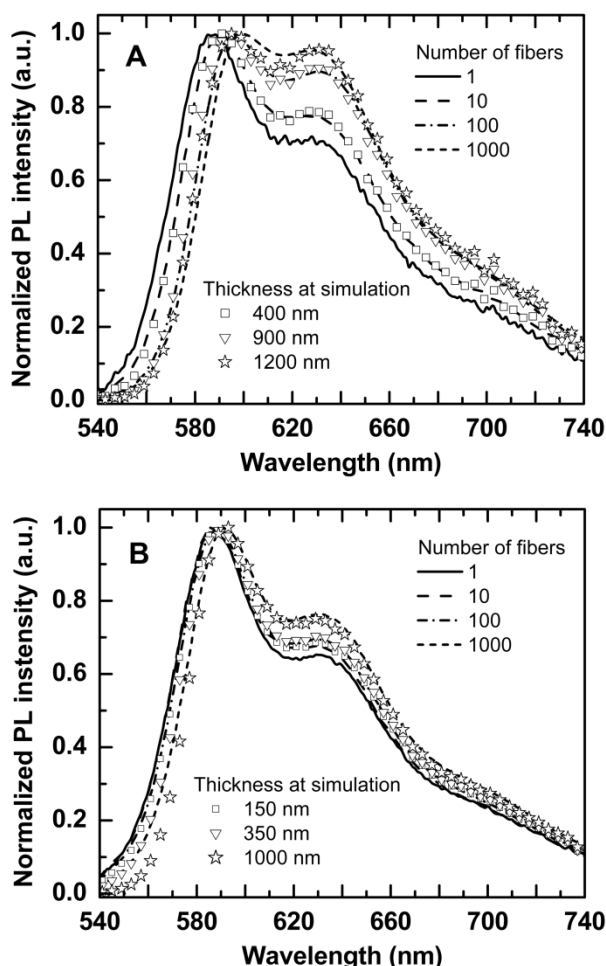
**Fig. 10** Normalized PL spectra simulated considering re-absorption and scatterings at different film thicknesses (plots) and normalized PL spectra of different numbers of electrospun fibers (lines): A) MEH-
5 PPV/PEO(HMW)/LiCF$_3$SO$_3$ and B) MEH-PPV/PEO(LMW) with twofold post-drawing. The simulations were performed using UV-vis absorption spectra measured without an integrating sphere.

## PL spectra from single fibers

   We have reported highly polarized PL from undrawn MEH-
10 PPV/PEO(LMW) electrospun nanofibers and enhanced PL polarization due to post-drawing[8]. Hence, MEH-PPV chains must be oriented to the fiber direction inside the nanofibers. PL spectra also give us significant information to understand the aggregation states and the electronic states of MEH-PPV chains inside the
15 electrospun nanofibers if we employ the PL spectra of a single fiber. Figure 13A shows the normalized PL spectra of a MEH-PPV/PEO(HMW)/LiCF$_3$SO$_3$ single fiber and spin-coated films with average thicknesses of 381 and 313 nm. Since re-absorption of PL occurs in the case of films and peak positions of the PL
20 changes, we have to carefully choose the film thicknesses [33]. A spin-coated film with a thickness of 381 nm was chosen since the thickness is comparable with the average diameter of the fibers (399 nm). In addition, a spin-coated film with a thickness of 313 nm was also chosen since the thickness is comparable with the
25 thickness of $h_0$; $h_0$ is a calculated value that assumes that the cross-sectional area ($S_0$) of the single fiber is equal to $S_0$ of a film when spread in a vertical direction to the fiber axis within the average diameter ($D$) of the single fibers (Fig. 13B). The equation
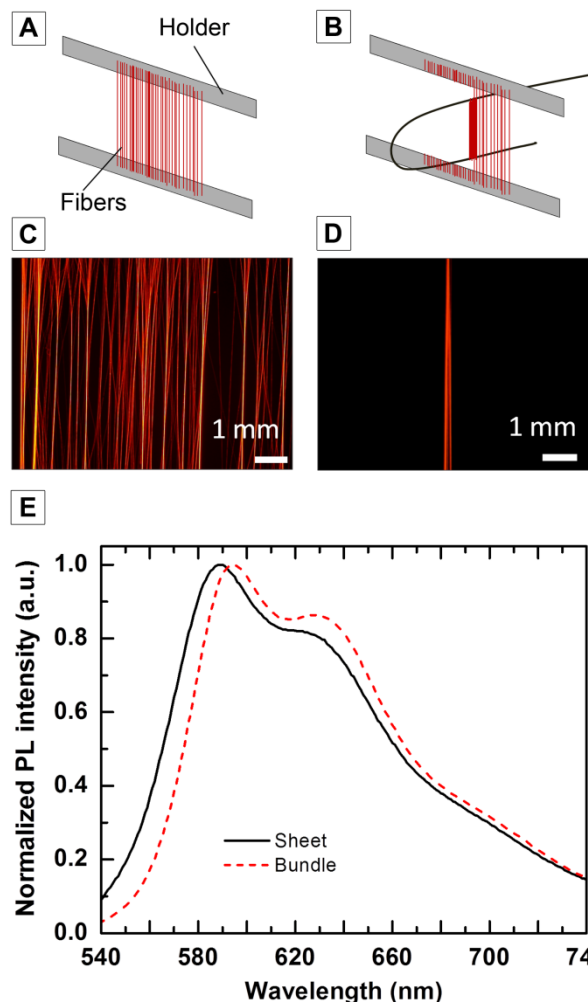


30 **Fig. 11**  A) Schematic illustration and C) fluorescent microscope image of a sheet of 1000 MEH-PPV/PEO(LMW) electrospun fibers with two-fold drawing. The sheet of the fibers was collected up forming a bundle. B) Schematic illustration and D) fluorescent microscope image of the
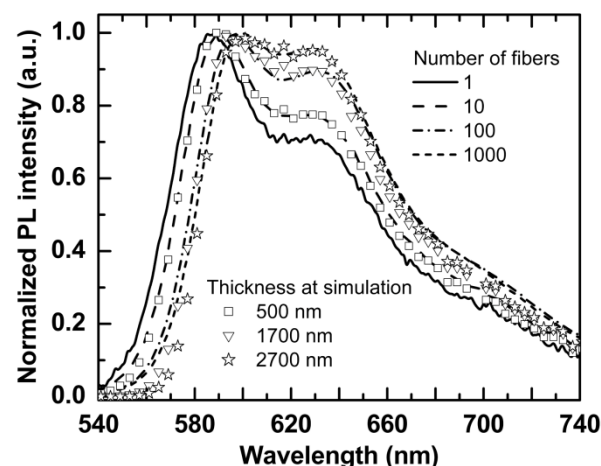35 bundle. E) Normalized PL spectra of the sheet and bundle.



**Fig. 12** Normalized PL spectra simulated using UV-vis absorption spectra of MEH-PPV/PEO(HMW)/LiCF$_3$SO$_3$ spin-coated films measured with an integrating sphere (plots) and normalized PL spectra of different numbers
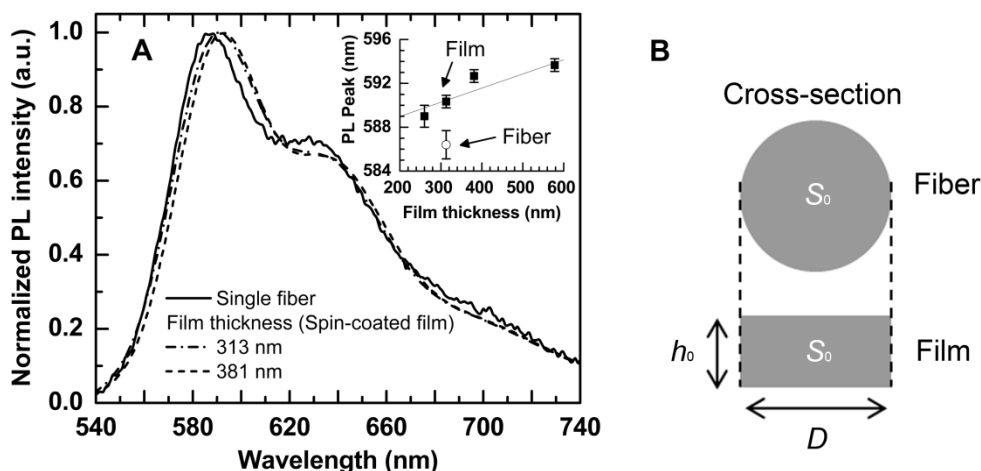40 of the electrospun fibers (lines).

**Fig. 13 A)** Normalized PL spectra of a single MEH-PPV/PEO(HMW)/LiCF$_3$SO$_3$ fiber and spin-coated films with different film thicknesses. Inset shows average maximum PL wavelengths of the spin-coated films as a function of film thickness. Average maximum PL wavelength of the single fibers was also plotted at a thickness of 313 nm. Errors reflect standard deviations. B) Schematic illustration of converting $D$ to $h_0$.
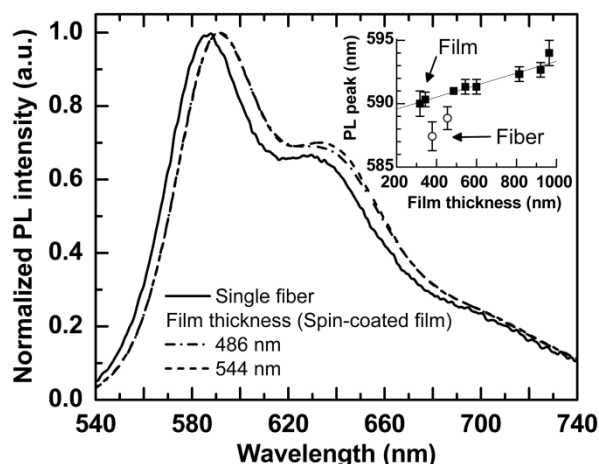


**Fig. 14** Normalized PL spectra of a single MEH-PPV/PEO(LMW) fiber with twofold post-drawing and spin-coated films with different film thicknesses. Inset shows average maximum PL wavelengths of the spin-coated films as a function of film thickness. Average maximum PL wavelength of the single fibers was also plotted at a thickness of 455 nm for undrawn fibers and 379 nm for twofold drawn fibers. Errors reflect standard deviations.

can then be described as follows: $S_0 = \pi D^2/4 = Dh_0$. Since $D$ is 399 nm, $h_0$ was calculated to be 313 nm, which is 78.5% of $D$. We calculated the average maximum PL wavelength by measuring ten individual fibers and three spin-coated films, which are plotted in the insets of Fig. 13A. The maximum PL wavelength of single fibers was blue-shifted compared to that of the spin-coated films: 6.3 and 3.9 nm with the thicknesses of 381 and 313 nm respectively. In addition, the PL spectra from the single fibers showed narrower spectra at around 590 nm than the spectra from the spin-coated films. This would be due to the smaller aggregation of MEH-PPV chains inside the electrospun fibers than those in the spin-coated films originated from geometrical confinement [34-37], or change of electronic states in ordered MEH-PPV chains.

Hagler *et al*. demonstrated tensile drawing of blend films of MEH-PPV/polyethylene, and after the tensile drawing MEH-PPV chains are highly aligned to the drawing direction[29]. PL spectra of the films sharpened and blue-shifted after the tensile drawing. They suggested this sharpening is due to improved electronic structure induced by alignment of the MEH-PPV chains. As mentioned at the beginning of this chapter, MEH-PPV chains are aligned to the fiber direction inside the electrospun nanofibers. Then, improved structural order of MEH-PPV chains leading to ordered electronic states would also occur inside the fibers. As for PL blue-shift, it was attributed to reduced stokes shift induced by the improved structural order. In the present study, we also observed blue-shift and sharpening of PL spectra for the fibers compared to the spin-coated film. The improved structural order and resulting ordered electronic states would be one of the reasons for blue-shift and sharpening of PL spectra. The relative PL intensity at wavelengths of around 630 and 700 nm for the single fiber was higher than that of the spin-coated films. This result was observed for all of the ten single fibers. Since emissions at around 630 and 700 nm are believed to originate from the interchain interactions among MEH-PPV chains [15-17], stronger interaction takes place in the MEH-PPV/PEO(HMW)/LiCF$_3$SO$_3$ electrospun fibers.

We also compared PL spectra of single MEH-PPV/PEO(LMW) fibers with twofold post-drawing to those of the spin-coated films with average thicknesses of 486 and 344 nm (Fig. 14). The thickness of 486 nm was comparable to the average diameter of the two-fold drawn fibers, and the thickness of 344 nm was comparable to $h_0$. The average maximum PL wavelength of the two-fold drawn single fibers was blue-shifted compared to the spin-coated films: 3.6 nm and 2.9 nm with the thicknesses of 486 and 344 nm, respectively (inset in Fig. 14).
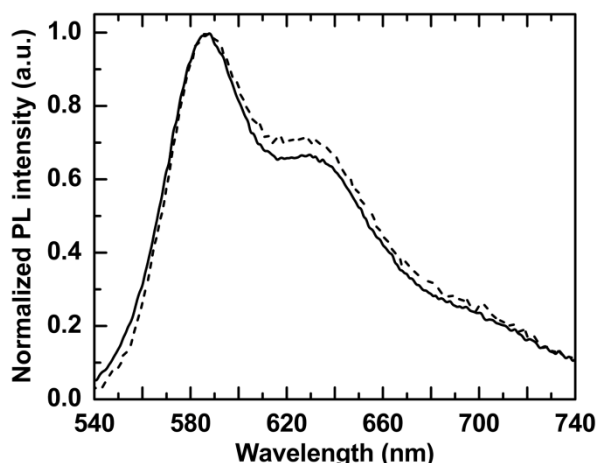
**Fig. 15** Normalized PL spectra of undrawn single MEH-PPV/PEO(HMW)/LiCF$_3$SO$_3$ fiber (dashed) and two-fold drawn MEH-PPV/PEO(LMW) single fiber (solid).

Compared to undrawn single fiber, the maximum PL wavelength of the two-fold drawn fibers was blue-shifted by 1.4 nm (inset in Fig. 14). The relative PL intensity at around 630 and 700 nm of the post-drawn single fibers was lower than that of the spin-coated films. Therefore, interchain interactions among MEH-PPV chains were lower in the MEH-PPV/PEO(LMW) electrospun fibers with twofold post-drawing compared to the spin-coated films. This would be due to weakened interchain interaction among MEH-PPV chains reported in drawn blend films of polyethylene and conjugated polymers[29, 38].

Finally, we compared PL spectrum of the undrawn single MEH-PPV/PEO(HMW)/LiCF$_3$SO$_3$ fiber with that of two-fold drawn single MEH-PPV/PEO(LMW) fiber (Fig. 15). The PL spectrum of the MEH-PPV/PEO(HMW)/LiCF$_3$SO$_3$ fiber showed higher relative intensity at wavelength of around 630 nm than that of the MEH-PPV/PEO(LMW) fiber, which indicates higher interchain interaction among MEH-PPV chains inside the MEH-PPV/PEO(HMW)/LiCF$_3$SO$_3$ fiber than that inside the MEH-PPV/PEO(HMW) fiber. This would be due to attraction originated from chemical doping effect of LiCF$_3$SO$_3$. Alternatively, it would be due to better interchain mixing between MEH-PPV chains and PEO(LMW) chains inside the MEH-PPV/PEO(LMW) fiber compared to the MEH-PPV/PEO(HMW)/LiCF$_3$SO$_3$ fiber because of the lower molecular weight PEO.

## Conclusions

We found that different number of electrospun fibers show different PL spectra. Simulation of the PL spectra using UV-vis absorption spectra measured with and without an integrating sphere suggests that the change in PL spectra is due to re-absorption and scatterings of PL among the fibers, namely, the properties of conjugated polymer chains cannot be deduced using the collective response of a mat, a sheet or a bundle. By comparing the PL spectra of isolated single nanofibers, we are able to deliberate the aggregation states and electronic states of nanoconfined conjugated polymer chains.

## Notes and references

*School of Materials Science, Japan Advanced Institute of Science and Technology (JAIST), 1-1 Asahidai, Nomi, Ishikawa 923-1292, Japan. Fax: +81-761-51-1149; Tel: +81-761-51-1531; E-mail: murata-h@jaist.ac.jp*

1.  M. V. Kakade, S. Givens, K. Gardner, K. H. Lee, D. B. Chase and J. F. Rabolt, *J. Am. Chem. Soc.*, 2007, **129**, 2777-2782.
2.  T. Kongkhlang, K. Tashiro, M. Kotaki and S. Chirachanchai, *J. Am. Chem. Soc.*, 2008, **130**, 15460-15466.
3.  L. M. Bellan and H. G. Craighead, *Polymer*, 2008, **49**, 3125-3129.
4.  K. H. K. Chan, T. Yamao, M. Kotaki and S. Hotta, *Synth. Met.*, 2010, **160**, 2587-2595.
5.  B. Dong, L. Gwee, D. Salas-de la Cruz, K. I. Winey and Y. A. Elabd, *Nano Lett.*, 2010, **10**, 3785-3790.
6.  S. W. Lee, H. J. Lee, J. H. Choi, W. G. Koh, J. M. Myoung, J. H. Hur, J. J. Park, J. H. Cho and U. Jeong, *Nano Lett.*, 2010, **10**, 347-351.
7.  D. Tu, S. Pagliara, A. Camposeo, L. Persano, R. Cingolani and D. Pisignano, *Nanoscale*, 2010, **2**, 2217.
8.  M. Campoy-Quiles, Y. Ishii, H. Sakai and H. Murata, *Appl. Phys. Lett.*, 2008, **92**, 213305.
9.  C. C. Kuo, C. T. Wang and W. C. Chen, *Macromol. Mater. Eng.*, 2008, **293**, 999-1008.
10. V. Vohra, U. Giovanella, R. Tubino, H. Murata and C. Botta, *ACS Nano*, 2011, **5**, 5572-5578.
11. H. C. Yang, T. J. Shin, L. Yang, K. Cho, C. Y. Ryu and Z. N. Bao, *Adv. Funct. Mater.*, 2005, **15**, 671-676.
12. Y. Shi, J. Liu and Y. Yang, *J. Appl. Phys.*, 2000, **87**, 4254-4263.
13. A. Kumar, M. A. Baklar, K. Scott, T. Kreouzis and N. Stingelin-Stutzmann, *Adv. Mater.*, 2009, **21**, 4447-4451.
14. G. He, Y. Li, J. Liu and Y. Yang, *Appl. Phys. Lett.*, 2002, **80**, 4247-4249.
15. T. Q. Nguyen, I. B. Martini, J. Liu and B. J. Schwartz, *J. Phys. Chem. B*, 2000, **104**, 237-255.
16. T.-Q. Nguyen, B. J. Schwartz, R. D. Schaller, J. C. Johnson, L. F. Lee, L. H. Haber and R. J. Saykally, *J. Phys. Chem. B*, 2001, **105**, 5153-5160.
17. S. H. Chen, A. C. Su, H. L. Chou, K. Y. Peng and S. A. Chen, *Macromolecules*, 2004, **37**, 167-173.
18. M. Campoy-Quiles, Y. Kanai, A. El-Basaty, H. Sakai and H. Murata, *Org. Electron.*, 2009, **10**, 1120-1132.
19. Y. Ishii, H. Sakai and H. Murata, *Mater. Lett.*, 2008, **62**, 3370-3372.
20. Y. Ishii, H. Sakai and H. Murata, *Thin Solid Films*, 2009, **518**, 647-650.
21. Q. B. Pei, Y. Yang, G. Yu, C. Zhang and A. J. Heeger, *J. Am. Chem. Soc.*, 1996, **118**, 3922-3929.

22. J. H. Shin, N. D. Robinson, S. Xiao and L. Edman, *Adv. Funct. Mater.*, 2007, **17**, 1807-1813.

23. P. Matyba, K. Maturova, M. Kemerink, N. D. Robinson and L. Edman, *Nat. Mater.*, 2009, **8**, 672-676.

24. A. Manuel Stephan and K. S. Nahm, *Polymer*, 2006, **47**, 5952-5964.

25. W. E. Teo and S. Ramakrishna, *Nanotechnology*, 2005, **16**, 1878-1884.

26. D. H. Reneker, A. L. Yarin, H. Fong and S. Koombhongse, *J. Appl. Phys.*, 2000, **87**, 4531-4547.

27. X. Yan and M. Gevelber, *J. Electrost.*, 2010, **68**, 458-464.

28. T. Yoshioka, R. Dersch, M. Tsuji and A. K. Schaper, *Polymer*, 2010, **51**, 2383-2389.

29. T. W. Hagler, K. Pakbaz, K. F. Voss and A. J. Heeger, *Phys. Rev. B*, 1991, **44**, 8652.

30. K. Kaloian, B. Ayi, A. Taek, C. R. M., H. Hans-Heinrich and B. Christoph, *Macromolecules*, 2006, **39**, 8692-8698.

31. C. Soci, D. Comoretto, F. Marabelli and D. Moses, *Phys. Rev. B*, 2007, **75**.

32. C. Chun-Ching, H. Chun-Min, C. Yi-Hao and K. Changshu, *Opt. Express*, 2010, **18**, A174-A184.

33. S. Pagliara, A. Camposeo, R. Cingolani and D. Pisignano, *Appl. Phys. Lett.*, 2009, **95**, 263301.

34. C.-C. Kuo, Y.-C. Tung, C.-H. Lin and W.-C. Chen, *Macromol. Rapid Commun.*, 2008, **29**, 1711-1715.

35. C.-C. Kuo, C.-H. Lin and W.-C. Chen, *Macromolecules*, 2007, **40**, 6959-6966.

36. S. Madhugiri, A. Dalton, J. Gutierrez, J. P. Ferraris and K. J. Balkus, *J. Am. Chem. Soc.*, 2003, **125**, 14531-14538.

37. C. T. Wang, C. C. Kuo, H. C. Chen and W. C. Chen, *Nanotechnology*, 2009, **20**.

38. B. He, J. Li, Z. Bo and Y. Huang, *Macromolecules*, 2005, **38**, 6762-6766.